Supplementary Information

Table S1: 130 half-Heusler (HH) compounds, the IDs on MatHub-3d, calculation time (a 64-core computing node, specifically an AMD EPYC 7452 @2.35GHz), the number of configurations in the HH130 dataset, and κ_Ls (considering both three and four phonon interactions) of 80 HH compounds at 300 K

Compound	ID	MLIP calculation time (h)				Number of configurations	$\kappa_L^{3ph+4ph}$ ($W \cdot m^{-1} \cdot K^{-1}$)
		Sampling	Labeling	Training	Total		
BaSnSr	84506	4.75	150.63	13.85	169.2	307	1.50
CaSnSr	84525	4.29	97.77	9.38	111.4	267	2.23
KSnY	84484	6.20	182.21	20.76	209.2	277	1.30
NaSnY	84551	14.27	66.41	15.88	96.6	312	
BiCePd	84407	5.14	52.55	14.89	72.6	210	3.08
PtSnTh	84664	3.10	48.55	12.40	64.1	180	3.75
BiRhZr	84493	4.39	39.72	13.29	57.4	177	9.16
BaNaSb	84540	3.07	27.32	7.07	37.5	180	0.74
BaKP	84482	3.49	46.35	5.94	55.8	176	2.72
MgSnSr	84486	4.80	50.95	7.10	62.8	204	1.39
BiRhTi	84485	3.10	24.38	8.33	35.8	140	9.26
NiSnTh	84658	2.90	195.50	11.86	210.3	212	5.86
CaSiSr	84574	3.51	33.13	6.59	43.2	156	4.40
CaMgSn	84580	6.74	39.61	11.34	57.7	206	2.69
NbRhSn	84409	6.93	86.89	14.31	108.1	238	
AuScSn	84601	3.06	60.46	9.36	72.9	151	8.69
AuInZr	84523	5.83	28.97	9.87	44.7	135	8.68
PbPtZr	84522	4.47	42.66	17.46	64.6	260	6.79
BiNiY	84408	3.26	82.04	10.17	95.5	155	6.86
RhSbTh	84667	3.19	65.70	11.86	80.7	162	3.40
PtSnZr	84534	3.61	48.63	14.91	67.1	175	12.99
BiGdNi	84422	3.33	60.85	9.69	73.9	145	8.07
PdSnZr	84447	3.41	46.66	11.97	62.0	164	11.78
BiDyNi	84471	5.65	77.14	9.76	92.5	171	
HfPbPt	84541	4.97	31.12	22.10	58.2	249	
BiHoNi	84444	2.97	84.08	7.33	94.4	149	10.59
PbPtTi	84503	17.99	41.92	18.33	78.2	224	
NbPtTl	84563	25.09	81.58	36.76	143.4	354	
BiNiTm	84442	3.66	58.30	10.57	72.5	166	11.25
MgTlY	84564	36.89	78.34	44.82	160.1	505	
GeNbRh	84573	43.83	57.79	43.21	144.8	363	
AuGeSc	84514	3.40	33.76	10.89	48.1	170	11.29

InNbPt	84559	47.35	74.42	22.02	143.8	314	
BiNiSc	84424	10.38	50.38	8.41	69.2	187	
HfPtSn	84410	7.29	51.57	18.55	77.4	278	
CdSiSr	84513	2.37	29.15	4.82	36.3	148	1.03
HfPdSn	84460	9.11	44.40	15.79	69.3	240	
PtSnTi	84449	28.83	100.51	33.35	162.7	370	
BiCoZr	84473	6.78	65.24	14.62	86.6	210	
PdSnTi	84571	26.93	96.18	29.83	152.9	347	
GePtZr	84492	3.57	34.65	14.42	52.6	215	11.97
PtTaTl	84560	10.42	34.47	21.74	66.6	247	
GeRhTa	84505	4.47	20.15	18.67	43.3	262	
NiSnZr	84434	2.99	53.81	11.03	67.8	173	14.71
InPtV	84555	10.27	97.93	38.19	146.4	383	
MgScTl	84512	64.96	58.38	41.03	164.4	485	
HfNiPb	84519	3.23	35.99	12.11	51.3	224	12.88
GaNbPt	84530	5.37	46.41	21.37	73.2	306	
GeHfPt	84533	3.00	16.24	10.83	30.1	210	
CaCdSi	84567	6.34	40.24	24.95	71.5	277	2.76
HfNiSn	84445	4.29	63.30	14.91	82.5	258	
GePtTi	84458	13.60	29.16	29.21	72.0	310	
CoNbSn	84433	28.82	142.42	46.95	218.2	390	
NiSnTi	84406	25.07	63.74	24.58	113.4	349	
NbRuSb	84597	42.37	55.23	17.91	115.5	280	
GaPtTa	84554	8.72	31.35	48.51	88.6	376	
LaNiSb	84579	3.80	84.07	11.55	99.4	207	1.75
HfRhSb	84411	19.74	31.82	25.46	77.0	307	
AsCaNa	84581	14.66	33.19	25.96	73.8	324	
GeNiZr	84568	4.78	40.24	17.75	62.8	227	18.36
GaPtV	84526	7.40	40.11	18.42	65.9	220	16.39
InNiTa	84543	3.60	32.31	15.39	51.3	221	10.99
CoLaTe	84494	3.74	107.75	15.70	127.2	222	0.44
AsRhZr	84545	3.28	32.31	13.56	49.1	216	19.16
CoTlW	84483	18.08	54.95	26.97	100.0	281	
RuSbTa	84450	4.23	27.97	18.43	50.6	263	
NaSiY	84569	4.14	23.17	14.31	41.6	248	
AgCaP	84546	3.40	29.42	10.90	43.7	207	0.51
RuSbV	84428	6.88	57.15	25.44	89.5	299	13.22
CoSnV	84448	20.01	73.75	27.30	121.1	291	
DyPtSb	84431	5.35	37.24	20.08	62.7	242	4.75
CaNiTe	84499	3.77	43.38	11.26	58.4	192	0.81
HoPdSb	84456	3.45	41.06	12.43	56.9	220	6.38
PtSbSc	84479	4.61	39.02	18.77	62.4	244	9.85
ErPdSb	84416	4.66	45.06	16.18	65.9	236	6.88
PdSbSc	84593	4.19	34.22	17.11	55.5	206	11.54

PdSbTm	84430	4.37	37.41	16.70	58.5	228	7.15
AsHfRh	84586	6.71	33.22	40.68	80.6	384	
NiSbY	84440	2.76	68.54	10.56	81.9	201	8.01
AsRhTi	84487	5.36	26.71	20.69	52.8	269	27.14
GeNiTi	84542	6.03	33.54	22.11	61.7	326	
BiLiMg	84596	5.51	31.25	38.51	75.3	248	4.18
GaNiV	84583	6.00	43.29	23.53	72.8	289	15.58
NiSbTb	84467	3.64	70.66	13.08	87.4	210	7.47
DyNiSb	84453	2.99	58.25	9.70	70.9	197	7.73
OsTeTi	84538	7.49	45.01	36.03	88.5	311	17.78
HoNiSb	84438	4.47	123.96	15.58	144.0	251	8.31
ErNiSb	84423	2.76	67.99	7.14	77.9	183	8.64
NiSbTm	84414	3.69	59.30	12.29	75.3	218	8.53
PtSiZr	84481	3.35	24.94	13.89	42.2	207	11.72
NiSbSc	84432	3.48	42.85	12.11	58.4	204	12.12
LuNiSb	84425	4.50	93.96	14.48	112.9	239	9.20
PdSiZr	84509	4.67	32.07	21.98	58.7	242	18.49
CoSbZr	84436	5.40	55.78	20.16	81.3	251	21.83
FeTeZr	84566	4.53	55.64	16.16	76.3	216	18.52
AgLiTe	84557	4.91	24.71	14.82	44.4	220	1.29
AlNbPt	84570	5.24	47.34	25.83	78.4	312	
CoScTe	84496	3.83	51.02	13.77	68.6	210	12.39
NiPY	84508	2.99	51.79	12.85	67.6	204	2.78
MgSiSr	84535	4.18	21.62	13.96	39.8	214	2.94
FeNbSb	84427	6.74	63.92	27.84	98.5	317	
LiNaTe	84495	9.09	20.09	15.26	44.4	333	
HfPtSi	84575	8.14	20.35	20.45	48.9	286	
AlPtTa	84561	4.39	13.75	9.59	27.7	194	
CoHfSb	84466	4.38	37.47	19.58	61.4	268	
AsCaLi	84517	3.38	17.91	14.81	36.1	236	2.60
PtSiTi	84498	5.37	29.02	25.96	60.4	297	
CoSbTi	84609	5.56	30.01	14.86	50.4	206	22.28
FeTeTi	84539	5.30	40.72	26.67	72.7	272	24.39
PdSiTi	84510	15.31	31.98	38.75	86.0	337	
AsCoZr	84488	3.21	35.59	14.19	53.0	210	19.76
FeSbTa	84584	4.15	29.69	17.02	50.9	222	
FeSbV	84589	5.62	46.72	31.56	83.9	288	23.14
AgBZr	84489	2.58	18.51	8.77	29.9	148	14.56
NiPSc	84480	3.99	29.68	15.76	49.4	196	9.34
HfNiSi	84490	4.54	26.32	16.33	47.2	235	
CdLiP	84439	2.47	10.40	8.14	21.0	145	3.51
FeSeTi	84502	3.39	27.63	15.64	46.7	211	24.86
AsCoTi	84562	5.43	34.87	20.91	61.2	271	33.16
AlNiV	84537	6.99	44.38	33.29	84.7	294	

LiScSi	84511	3.81	15.50	12.43	31.8	212	20.40
AsLiZn	84446	3.54	14.39	13.96	31.9	185	3.81
GaLiSi	84426	7.01	10.69	35.91	53.6	324	
LiPZn	84472	5.47	13.99	21.53	41.0	249	5.63
MgNaP	84565	7.80	11.15	31.01	50.0	342	
LiNZn	84478	4.56	8.08	19.73	32.4	169	12.04
AsLiMg	84452	4.48	6.63	16.37	27.5	211	6.96
LiMgP	84590	3.71	5.28	15.47	24.5	217	6.52
AlLiSi	84417	6.30	6.62	29.39	42.3	280	
LiMgN	84527	4.93	5.22	31.25	41.4	250	

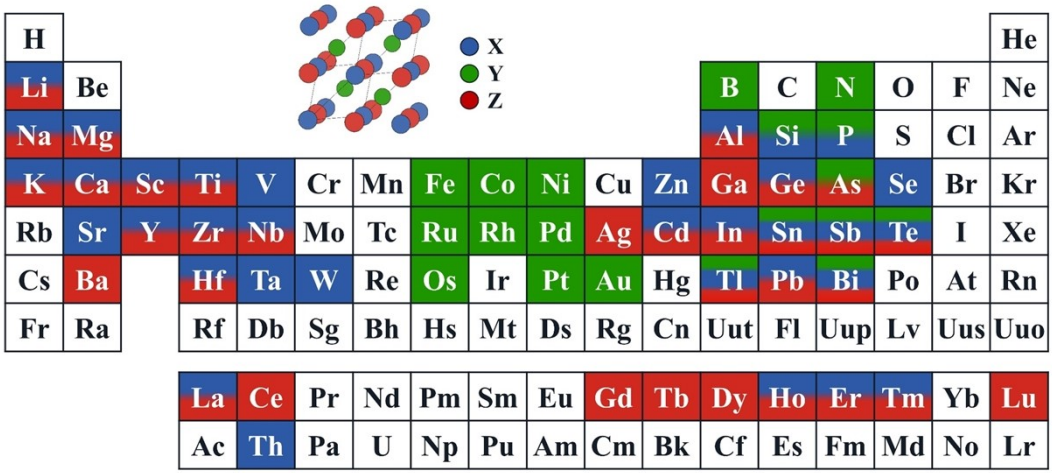

Figure S1: The crystal structure of half-Heusler and the elements considered in this study.

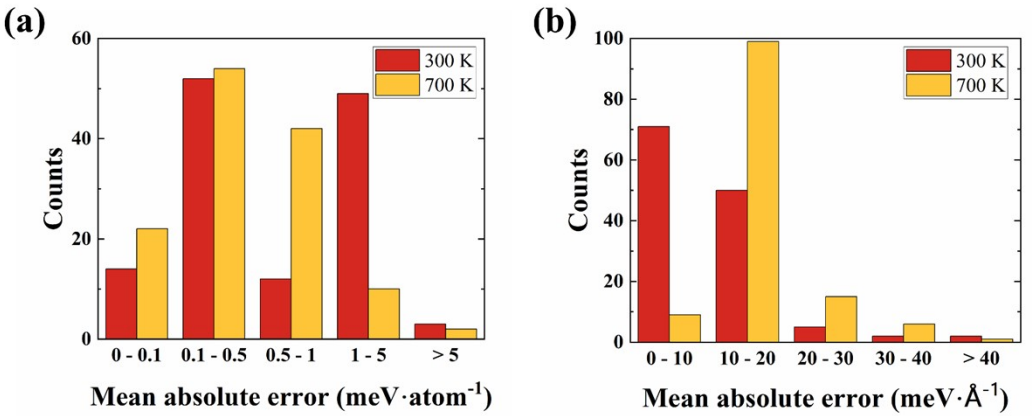

Figure S2: The MAEs of (a) energies and (b) forces at 300 K (red bar) and 700 K (yellow bar) for 130 HH compounds.

Supplementary Note 1:

Testing the level and cutoff radius of the MTP model

To evaluate the training level of MTP models, three models were directly constructed using a comprehensive training dataset of 206 configurations of TiCoSb. The average training time and errors in energies and forces across all configurations were statistically analyzed. Level testing was conducted on a 24-core computing node, with two Intel® Xeon® Gold 6126 CPU @ 2.60 GHz, with all parameters unchanged except for the training level. As shown in Table S2, increasing the level from 16 to 18 resulted in a slight increase in training time and a reduction in errors. However, beyond level 18, further increments nearly doubled the training time while the rate of error reduction remained consistent. Therefore, a training level of 18 was deemed optimal for MTP models in this study.

Table S2: Evaluation of the MTP model training level for TiCoSb

Level	Training time (min)	MAEs of the energies ($meV \cdot atom^{-1}$)	MAEs of the forces ($meV \cdot Å^{-1}$)
16	76	2.524	9.75
18	87	2.521	8.53
20	155	2.520	7.44
22	329	2.515	6.70

The cutoff radius of the MTP model was tested on a 24-core computing node, with two Intel® Xeon® Silver 4310 CPUs @ 2.10 GHz. As shown in Table S3, increasing the radius from 5.5 Å to 6.0 Å resulted in minimal changes in both average training time and energy errors, with a slight reduction in force errors. However, beyond a radius of 6.0 Å, further increases led to a significant increase in training time, while the rate of reduction in force errors remained consistent. Additionally, considering the crystal structures of HH compounds and their atomic interaction ranges, we statistically analyzed the atomic nearest-neighbor distances for 130 HH compounds, finding average distances of 5.24 Å, 6.32 Å, and 6.88 Å for the third, fourth, and fifth nearest neighbors, respectively. Therefore, to balance computational efficiency and model

accuracy, selecting a 6.0 Å cutoff radius for training the MTP model is reasonable, as it effectively covers critical nearest-neighbor interactions while avoiding unnecessary computational costs.

Table S3: Evaluation of the MTP model cutoff radius for TiCoSb

Cutoff radius (Å)	Training time (min)	MAEs of the energies (meV·atom^{-1})	MAEs of the forces (meV·Å^{-1})
5.5	99	2.524	8.74
6.0	98	2.525	8.53
6.5	130	2.523	8.12
7.0	183	2.517	7.93

Supplementary Note 2:

Comparison of the efficiency of MLIP and DFT calculations

Table S4 presents the average time allocated to each phase of the high-throughput calculation for 130 HH compounds, including sampling, labeling, training, and total time. The computational resources utilized were a 64-core computing node, specifically an AMD EPYC 7452 @ 2.35 GHz. DFT labeling constitutes 64% of the total computational time, making it the most time-consuming component. On average, the entire MLIP process for each HH compound requires 75 hours, with the training dataset containing an average of 245 configurations.

Table S4: The time spent on each component in high-throughput calculations

Sampling time (h)	Labeling time (h)	Training time (h)	Total (h)
8	48	19	75

Based on the trained MLIP models, atomic forces can be directly obtained from small displacement structures, allowing for the rapid acquisition of high-order IFCs and a significant reduction in high-throughput computational costs. As shown in Table S5, the efficiency difference between DFT and MLIP is quantified by the number of DFT

calculations required. For a 192-atom HH supercell, considering the cutoff distance settings described in the main text, approximately 500 and 2000 DFT calculations are needed to obtain 3rd- and 4th-order IFCs, respectively. Using the average number of configurations in the training dataset as a reference (with an average of 245 static DFT calculations per HH compound), the entire process of training the MLIP model and obtaining 3rd-and 4th-order IFCs is estimated to require 383 DFT calculations. This is slightly fewer than the number of DFT calculations needed for 3rd-order IFCs alone. Incorporating 4ph scattering, the MLIP model reduces the originally required 2500 DFT calculations to only 383, resulting in a reduction in computational time by an IFC of magnitude.

Table S5: Estimation of the number of DFT calculations required for each process

3rd-order IFCs	4th-order IFCs	DFT Labeling	MLIP Process
500	2000	245	383

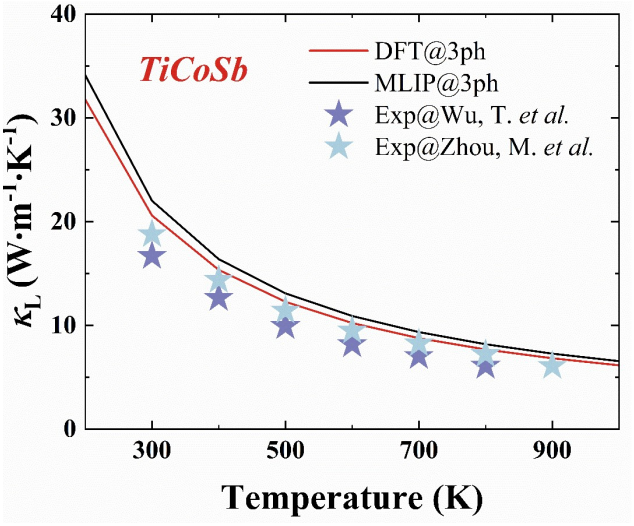

Figure S3: The κ_L of theoretical and experimental data for TiCoSb. Experimental data are taken from Wu *et al.*[1] and Zhou *et al.*[2]

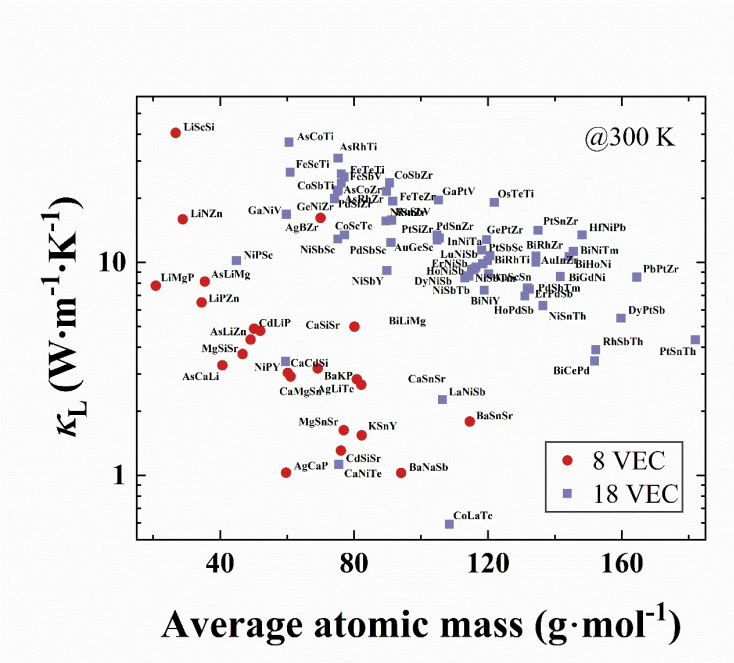

Figure S4: The relationship between the κ_L^{3ph} of 80 HH compounds with 8 (red plot) and 18 (blue-purple plot) VEC at 300 K and their average atomic mass.

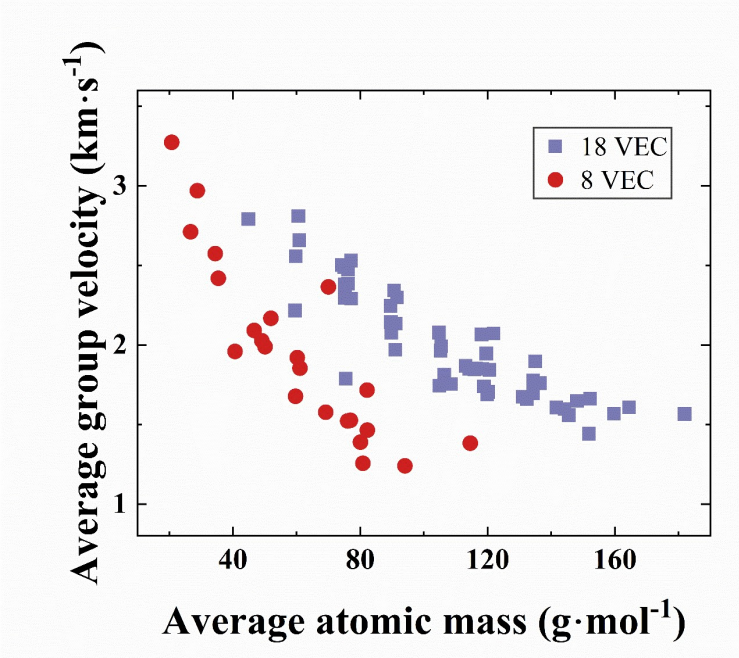

Figure S5: The relationship between the average group velocity of 80 HH compounds with 8 (red plot) and 18 (blue-purple plot) VEC and their average atomic mass.

Supplementary Note 3:

The methodology for averaging the 2nd-order IFCs

In this study, we calculated and ranked the magnitudes of all 2nd-order IFCs for each HH compound. Due to the significant influence of interatomic distances on atomic forces, the 2nd-order IFCs of the first few nearest neighboring atoms are significantly larger, typically one to two orders of magnitude greater than those of the next nearest neighbors. This disparity in magnitudes underscores the importance of considering the strongest interactions in the material. Consequently, we computed the equivalent average 2nd-order IFCs based on the three largest values, aiming to capture the most influential and dominant contributions to interatomic forces.

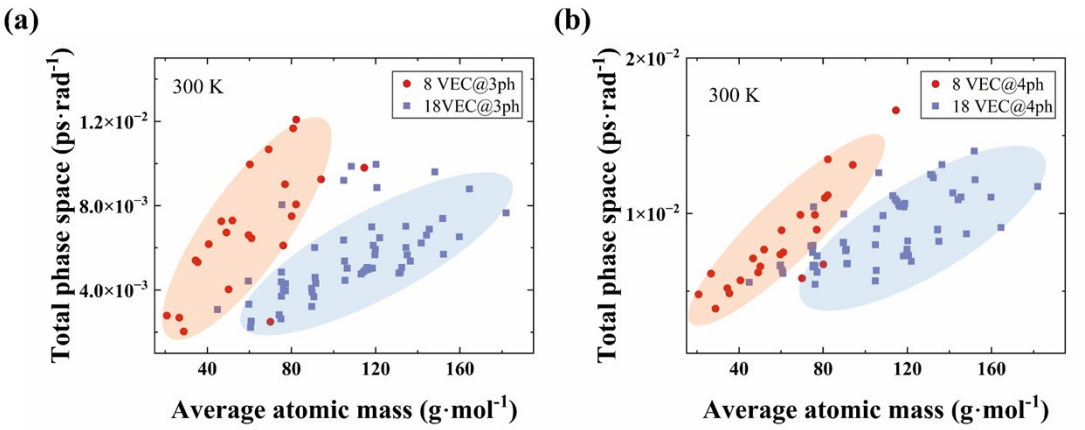

Figure S6: The relationship between the (a) 3ph and (b) 4ph total phase space of 80 HH compounds with 8 (red plot) and 18 (blue-purple plot) VEC at 300 K and the average atomic mass.

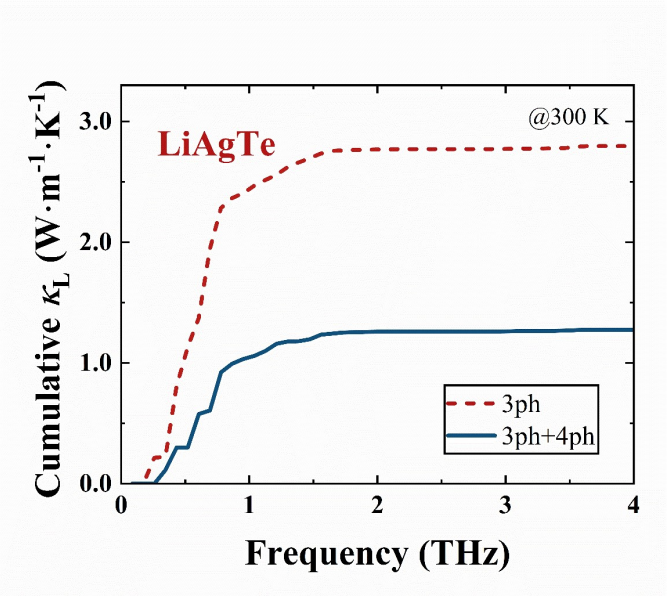

Figure S7: The cumulative κ_L for LiAgTe at 300 K as a function of frequency, with (blue line) and without (red dashed line) 4ph scattering.

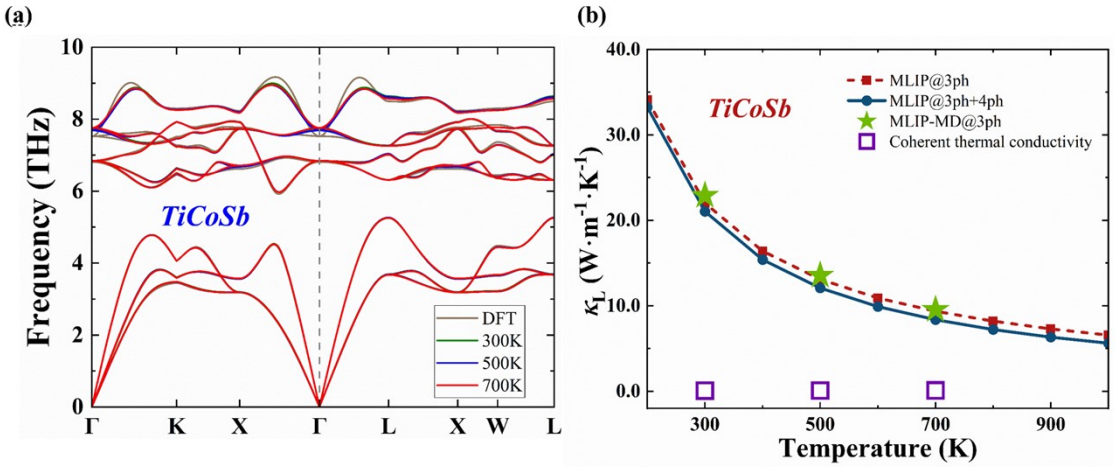

Figure S8: The impact of phonon renormalization at finite temperatures on (a) phonon dispersions, (b) lattice thermal conductivity results and coherent thermal transport effects for TiCoSb.

References

1. T. Wu, W. Jiang, X. Li, S. Bai, S. Liufu and L. Chen, *J. Alloys Compd.*, 2009, **467**, 590-594.
2. M. Zhou, L. Chen, C. Feng, D. Wang and J.-F. Li, *J. Appl. Phys.*, 2007, **101**, 113714.